Hindawi
Geofluids
Volume 2023, Article ID 5075888, 11 pages
https://doi.org/10.1155/2023/5075888

Research Article

The Time-Varying Variation Characteristics of Methane during Nitrogen Injection Process: An Experimental Study on Bituminous Coals

Aoxiang Zhang, Longyong Shu, Zhonggang Huo, and Xin Song

China Coal Research Institute, Beijing 100013, China

Correspondence should be addressed to Longyong Shu; slyccri@163.com

Received 8 May 2023; Revised 30 November 2023; Accepted 30 November 2023; Published 11 December 2023

Academic Editor: Kouqi Liu

The existing research on CH_4 displacement by N_2 mainly focuses on the gas injection displacement mechanism and the factors affecting displacement efficiency. And most of them are theoretical analyses at the model level or multifactor analyses at the simulation test level, while there are few targeted physical simulation tests and quantitative analyses. Given the above problems, the experiment system was used to study the gas migration evolution law and time-varying characteristics of CH_4 displacement by N_2 in coal under different injection pressures. The experimental results show that the whole process of CH_4 displacement by N_2 can be divided into three stages: stage I (original equilibrium stage); stage II (dynamic balance stage); stage III (new equilibrium stage). The concentration of CH_4 and N_2 presents an opposite variation trend, and the variation rate of CH_4 and N_2 increased first and then decreased. The breakthrough time was 50 minutes, 45 minutes, 35 minutes, 25 minutes, and 20 minutes, respectively, under different injection pressures. The displacement efficiency increased with the injection pressures, while the replacement ratio decreased with the injection pressures. The maximum flow rate of CH_4 was 0.085 mL/min, 0.110 mL/min, 0.130 mL/min, 0.222 mL/min, and 0.273 mL/min, respectively, under different injection pressures. The accumulated production of CH_4 was 3.59 mL, 3.91 mL, 4.39 mL, 5.58 mL, and 5.94 mL, respectively, under different injection pressures. The effective injection pressure range was 1.6~2 MPa. This research can provide a reference for the theoretical research of N_2-ECBM-related technology in low permeability reservoirs and the selection of injection pressure in the field technology implementation.

1. Introduction

Coalbed methane is a fossil energy associated with the natural evolution of coal [1]. The development of coalbed methane cannot only ensure the safe production of coal mines but also alleviate the increasingly severe energy crisis [2, 3]. Borehole gas extraction has become the main way to prevent gas disasters and develop coalbed methane [4–6]. Coal seams are a dual porous medium composed of coal matrix blocks and interblock fractures [7, 8]. The adsorbed gas and the free gas in the cracks reach equilibrium under a certain pressure [9]. The extraction drilling hole can form a gas pressure gradient, promoting the free gas in the fractures to flow towards the drilling hole [10–12]. With the extension of the extraction time, the gas pressure in the coal seam fractures gradually decreases [13]. The dynamic equilibrium between the adsorbed gas and the free gas is broken, and the adsorbed gas is desorbed and diffused from the matrix to the fractures [14, 15]. However, with the progress of gas extraction, the gas pressure gradient between the coal seam and the borehole also gradually decreases [16–18].

Conventional enhanced extraction technology can be divided into three categories: mechanical methods, physical methods, and chemical methods [19–22]. The physical properties of coal and external technology in this process are transformed and utilized, which constitutes the main content of the enhanced extraction technology [23–25]. However, low permeability, low reservoir pressure, and low

gas content are the characteristics of coal reservoirs in China. Conventional enhanced extraction technologies are not effective in this type of reservoir. Due to its particularity, gas injection technology can effectively improve the gas extraction efficiency by increasing the gas driving force and reducing the effective stress and the gas partial pressure [26]. Thus, the gas injection technology can rapidly reduce the gas content in the coal seam and ensure mining safety.

There have been several theoretical and experimental studies on gas injection technology. Longinos et al. examined the efficacy of liquid nitrogen in the coal fracturing process in coalbed methane reservoirs [27–29]. Wu et al. developed a dual pores model for enhanced methane recovery by CO_2 injection [30]. Kumar et al. developed a coupled finite element (FE) model to study the heterogeneously permeable coal reservoirs [31]. Ozdemir established a mixed-gas-coupled seepage model of porous media, taking into account the effect of moisture in coal [32]. Huang et al. established a water-gas two-phase coupled seepage model which considered the influence of water on gas seepage [33]. Seto et al. established a gas-water two-phase flow model which considered the interaction of gases (CO_2, N_2, CH_4, and H_2O) in the coal seam [34]. Xia et al. used a coupled composition model to study the effect of borehole sealing on gas emissions [35]. There are also several field trials of enhanced methane recovery involving gas injection. The United States conducted CO_2-ECBM test and N_2-ECBM test at the Allison Unit and Tiffany Unit, respectively [36]. Canada had conducted a gas injection test for CO_2 storage in Alberta Province [37]. The European Union's RECOPOL project was first implemented in Poland, with a gas injection depth of 1050 m [38]. Japan had conducted a field test of gas injection to replace coalbed methane in Hokkaido [39, 40]. China and Canada jointly carried out a study that focused on the recovery enhancement of coalbed methane in the Qinshui Basin, Shanxi Province [41, 42].

In this paper, we investigated the gas migration law and time-varying characteristics of CH_4 displacement by N_2 in coal under different injection pressures by a physical simulation experiment. Based on the above results, this research can provide a reference for the theoretical research of N_2-ECBM-related technology in low permeability coal seams and the selection of injection pressure in the field technology implementation.

2. Materials and Methods

2.1. Sample Collection and Preparation. The raw coal samples were collected from the Tashan mine in Shanxi, China. The raw coal samples were made into cylindrical coal samples with specifications of 50 mm in length and 25 mm in diameter. The raw coal and cylindrical coal samples are shown in Figure 1.

2.2. Experimental Equipment. The experiment uses HA-I multiphase flow permeameter test device (Figure 2). Its main technical parameters include (1) maximum working pressure: annular pressure: 25 MPa, accuracy: ±0.01 MPa; injection pressure: 20 MPa, accuracy: 0.01 MPa; ring pressure: 20 MPa, accuracy: ±0.01 MPa; (2) maximum working temperature: 120°C, accuracy: ±0.1°C; and (3) specification of the core holder: 25 mm, 50 mm, and 60 mm (diameter).

The instrument mainly includes the following systems: (1) core clamping system: the core is wrapped by polytetrafluoroethylene casing; (2) gas injection system: gas can be injected into the core holder under constant pressure; (3) pressure system: the back pressure is controlled by the back pressure valve, and the annular pressure is the pressure loaded around the core by the injection pump; (4) data metering system: the inlet and outlet ends of the core holder are, respectively, equipped with a pressure sensor for real-time monitoring of the pressure values at both ends, and the gas component detector and drainage method are used to measure the flow rate of the mixed gas; (5) temperature control system: temperature control adopts thermostat air bath heating, temperature range: 20°C~120°C. The schematic diagram of the device is shown in Figure 3.

2.3. Experimental Scheme. The influence of different injection pressures on the process of CH_4 displacement by N_2 was analyzed. The standard coal sample size is 25 × 50 mm. The experiment adopts a true triaxial loading: the confining pressure is 4.0 MPa, and the axial pressure is 2 MPa. The adsorption pressure of CH_4 is 1 MPa, and the adsorption time is 24 h, which ensures that the pressure remains stable and the flow remains unchanged within 30 min when the adsorption is saturated. The N_2 injection pressure is within the range of 0.5~2.5 MPa, and the ambient temperature is set at 25°C. Specific experimental parameters are shown in Table 1.

2.4. Experimental Procedures. The following are the experimental operation steps: (1) replace the test sample with a solid cushion block, connect the instrument, and check the air tightness of the test device; (2) put the coal sample (25 × 50 mm) into the holder; (3) add an axial pressure of 1 MPa first, and then the ring pressure of 2 MPa, and pressurize alternately step by step until the ring pressure is 4 MPa, and the axial pressure is 2 MPa; (4) vacuum the whole system for 2 hours; (5) inject 1 MPa methane into the holder through the pressurization system, close the downstream valve, and maintain it for 12 hours to ensure complete adsorption; (6) inject 0.5, 1, 1.5, 2, and 2.5 MPa nitrogen, respectively, open the downstream valve, and connect the gas detector to analyze the outlet gas concentration; (7) when measuring the flow, close the branch valve of the gas detector, open the flow valve, and measure the flow. Switch back to the gas detector branch in time after measurement; (8) collect the monitoring data, record the flow, and the gas detector shows that the concentration of each gas is not changing; (9) after the test, relieve the pressure step by step and disassemble the test device.

3. Results

3.1. Conversion Process of CH_4 Displaced by N_2. The displacement of CH_4 by N_2 is a dynamic process. The released gas volume changed constantly under different injection

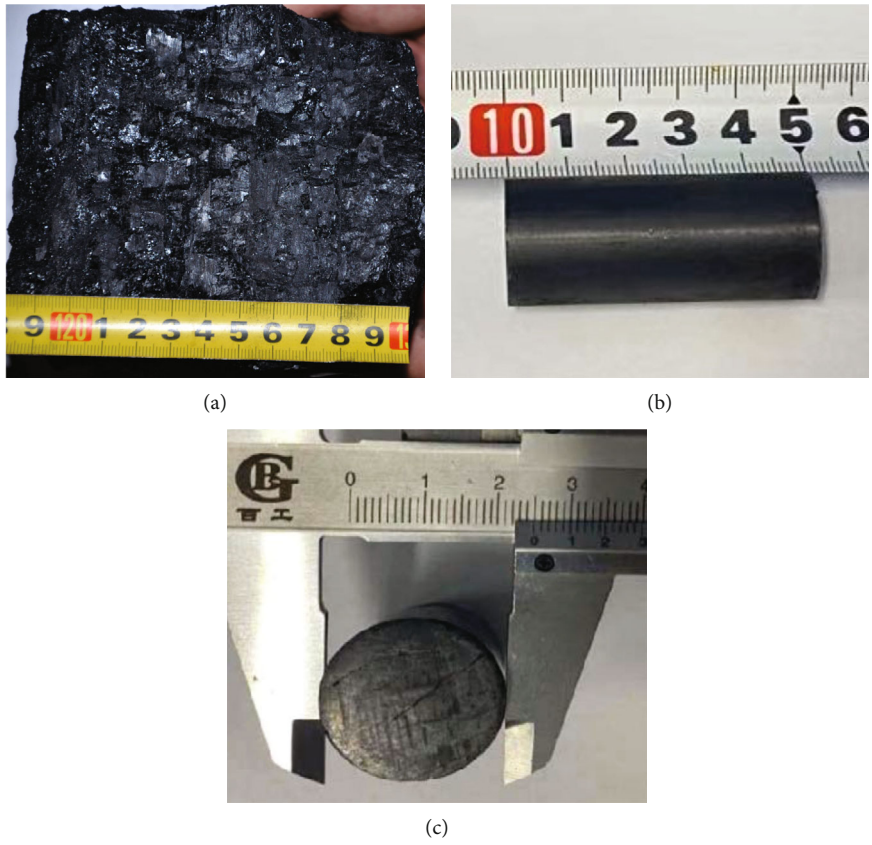

(a) (b) (c)

Figure 1: Experimental sample diagram: (a) raw coal sample, (b) front view columnar coal sample, and (c) sectional view of columnar coal sample.

pressures and injection times. The results show that the displacement of CH_4 by N_2 results from the joint action of multiple mechanisms. It can be seen from Figure 4 that the whole process can be divided into three stages (taking the injection pressure of 1.0 MPa as an example). Stage I (original equilibrium stage): the volume fraction of N_2 was 0, and the volume fraction of CH_4 was 100%. At first, N_2 was injected into the coal samples saturated with CH_4. The migration speed of N_2 through "seepage-diffusion-adsorption" under the pressure gradient is relatively slow. It takes a specific time to break the original equilibrium state. Stage II (dynamic balance stage): N_2 had seeped from fractures with continuous gas injection. Then, N_2 diffused into the pores of the coal matrix, and the concentration of N_2 began to increase while the concentration of CH_4 decreased. There was a dynamic change relationship of "this and the other." This is because the partial pressure of CH_4 decreased, and CH_4 is desorbed from the coal matrix after N_2 injection. In addition, the concentration difference between macropores and micropores will be increased with the migration of free CH_4 in fractures. Thus, the CH_4 desorption was accelerated. In this stage, CH_4 desorbed from the coal matrix and diffused to the fractures under the concentration gradient. Stage III (new equilibrium stage): the concentration of N_2 increased to 100%, while the concentration of CH_4 decreased to 0 with continuous N_2 injection. The new equilibrium state was established, and the CH_4 was no longer desorbed.

3.2. The Concentration Change of the Output Gas. It can be seen from Figures 5 and 6 that the concentrations of CH_4 and N_2 present an opposite variation trend, and the variation rate of CH_4 and N_2 increased first and then decreased. The results showed that the CH_4 concentration was 100% while the N_2 concentration was 0 in stage I. The duration of stage I was 50 minutes, 35 minutes, 25 minutes, 15 minutes, and 10 minutes, respectively, at the level of 0.5 MPa, 1 MPa, 1.5 MPa, 2 MPa, and 2.5 MPa. This indicated that the N_2 had not broken through the coal samples at this stage. Then, the CH_4 concentration gradually decreased. But the decrease rate of CH_4 concentration decreased in the 85th minute, 70th minute, 50th minute, 35th minute, and 25th minute, respectively, at the level of 0.5 MPa, 1 MPa, 1.5 MPa, 2 MPa, and 2.5 MPa. Finally, the CH_4 concentration decreased to less than 5% in the 100th minute, 80th minute, 60th minute, 40th minute, and 30th minute, respectively, at the level of 0.5 MPa, 1 MPa, 1.5 MPa, 2 MPa, and 2.5 MPa.

3.3. Breakthrough Time and Displacement Time. Breakthrough time refers to the time that the N_2 passes through the coal samples. The breakthrough time was an important index to evaluate the effect of CH_4 displacement by N_2. The seepage and diffusion of N_2 in the coal samples depended on the pressure gradient and concentration gradient. Due to the slow diffusion rate, the injection pressure played a crucial role in this process. At the initial stage of

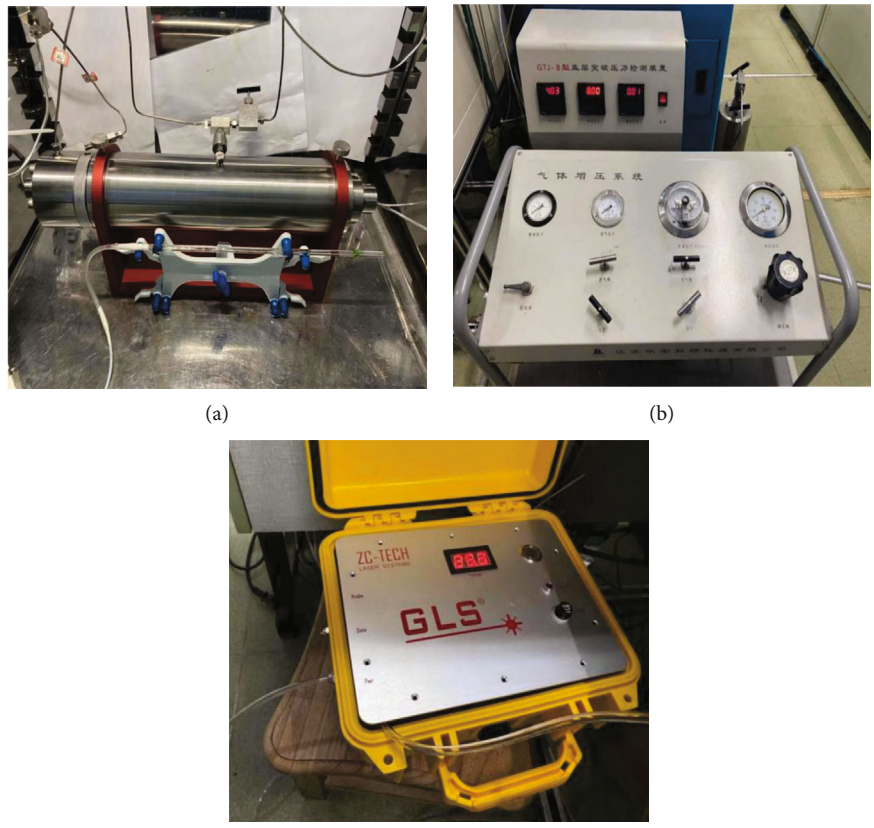

Figure 2: Diagram of main experimental equipment: (a) core holder, (b) pressurization system, and (c) gas component detector.

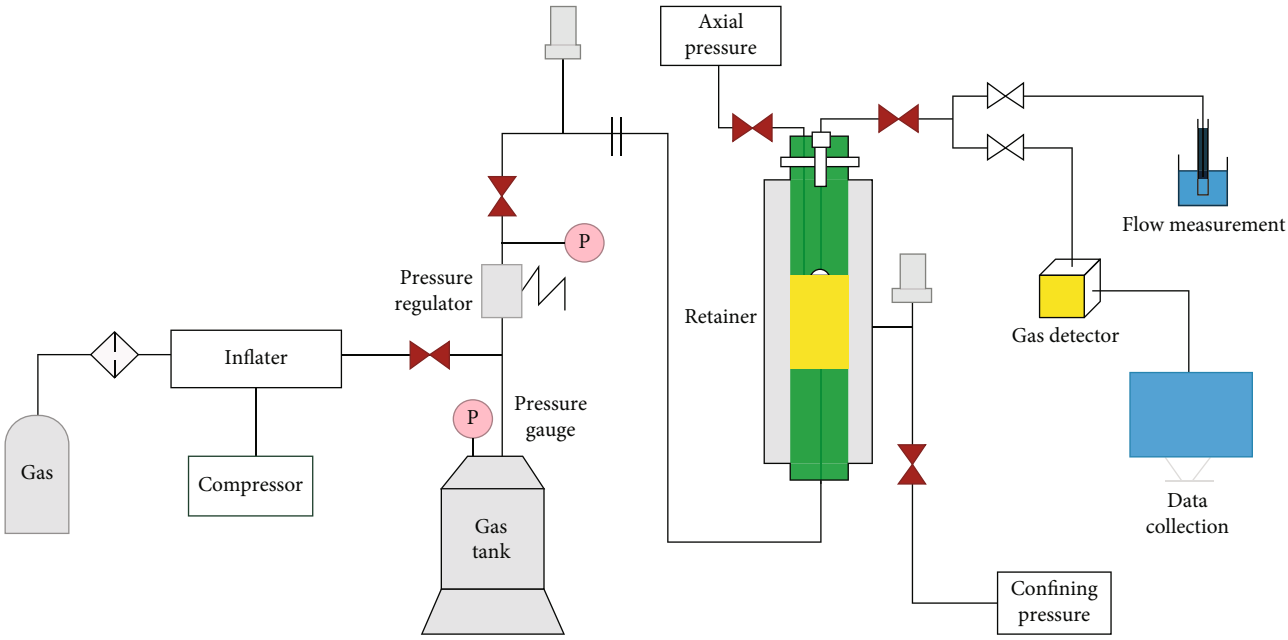

Figure 3: Flow chart of the experimental device.

N_2 injection, the N_2 will remain in the coal samples and cannot be detected at the outlet. It can be seen from Figure 7 that the breakthrough time was 50 minutes, 45 minutes, 35 minutes, 25 minutes, and 20 minutes, respectively, at the level of 0.5 MPa, 1 MPa, 1.5 MPa, 2 MPa, and 2.5 MPa. In this process, the breakthrough time decreased by 10%, 30%, 50%, and 60%, respectively, with the increase in injection pressure. It can be concluded that the breakthrough

Table 1: Experimental parameters of CH_4 displacement by N_2.

Code	Displacement pressure (MPa)	Sample size (mm)	CH_4 adsorption pressure (MPa)	Confining pressure (MPa)	Axial pressure (MPa)	Temperature (°C)
1	0.5	25 × 50	1	4	2	20
2	1	25 × 50	1	4	2	20
3	1.5	25 × 50	1	4	2	20
4	2	25 × 50	1	4	2	20
5	2.5	25 × 50	1	4	2	20

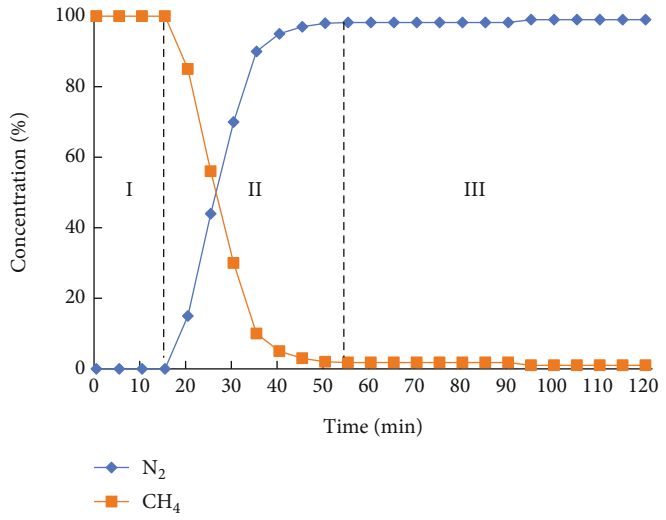

Figure 4: Variation of concentration with gas injection time.

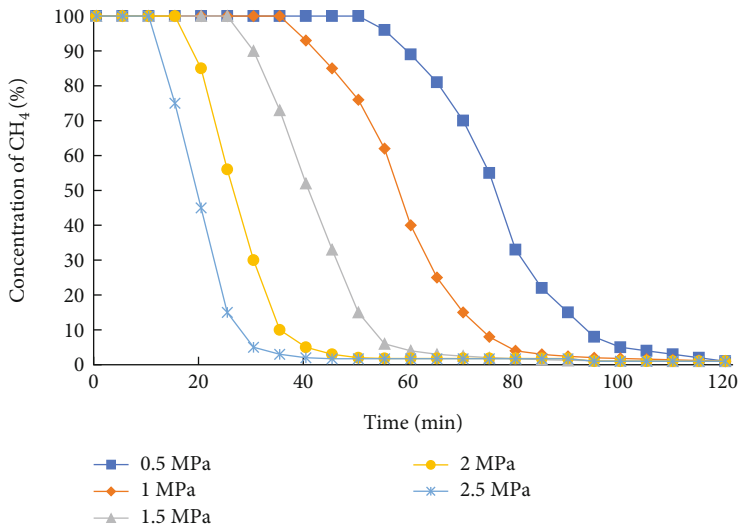

Figure 5: Variation of CH_4 concentration under different pressures.

time was gradually shortened and the change rate decreased with the increase of injection pressure. At this stage, the N_2 would diffuse into the micropores and occupy the adsorption vacancy in the coal surface. At this time, the seepage process was not dominant. Then, the seepage velocity of N_2 in the fractures increased with the increase of N_2 injection pressure. Thus, the seepage velocity was faster than the diffusion velocity result in that the seepage process was dominant. Therefore, the N_2 would pass through the coal samples rapidly.

Displacement time refers to the time that the concentration of CH_4 decreased from 100% to a particular value in the

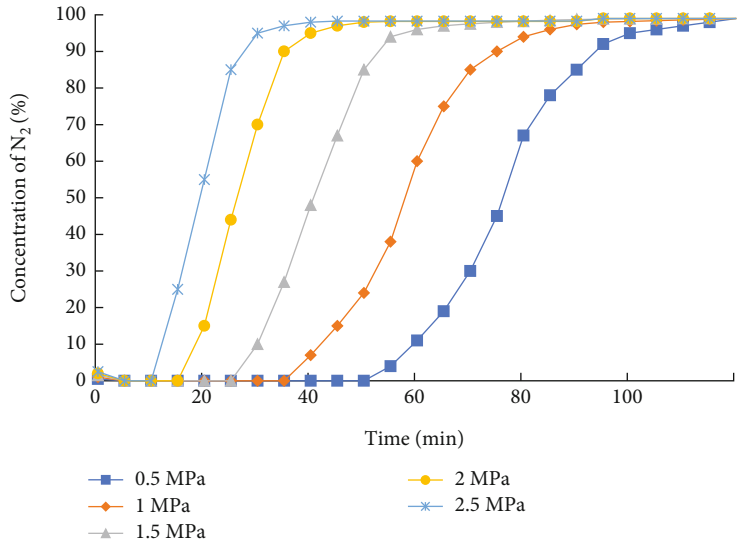

Figure 6: Variation of N_2 concentration under different pressures.

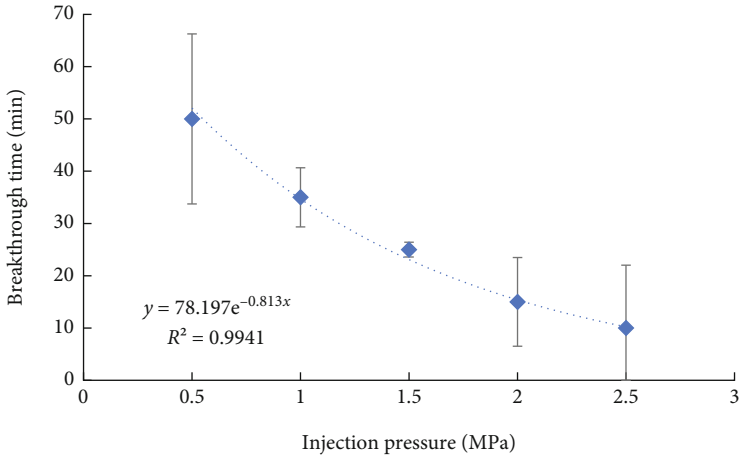

Figure 7: Breakthrough time under different pressures.

injection process. It can be seen from Figure 8 that the displacement time was 5 minutes at the level of 2.5 MPa, while the displacement time was 35 minutes at the level of 0.5 MPa. This indicated that the higher the injection pressure, the faster the variation of the CH_4 concentration. The results showed that the pressure gradient between the inlet and the outlet of the coal sample increased with the increase of injection pressure. Thus, the gas was easier to migrate. On the other hand, the high pore pressure offsets part of the effective stress, which reduced the pressure on the coal skeleton. Then, the porosity increased. Thus, the permeability of the coal sample was increased so that the gas migration velocity was accelerated.

3.4. Displacement Efficiency and Replacement Ratio. According to the total mixed flow q of CH_4 and N_2 measured under different injection pressures and different gas volume fractions (φ_{CO2}, φ_{CH4}), the output of CH_4 and N_2 can be calculated. Finally, the displacement efficiency η and replacement ratio μ under different pressure conditions are obtained. The calculation formula is as follows:

$$\eta = \frac{Q_{CH_4}}{Q^T_{CH_4}} \times 100\% = \frac{\int_0^t \varphi_{CH_4} q dt}{Q^T_{CH_4}} \times 100\%,$$
$$\mu = \frac{Q^T_{N_2}}{Q_{CH_4}} \times 100\% = \frac{Q^T_{N_2}}{\int_0^t \varphi_{CH_4} q dt} \times 100\%, \quad (1)$$

where η is the efficiency of N_2 displacing CH_4 (%); Q_{CH4} is CH_4 output (mL); $Q^T{}_{CH4}$ is the total injection amount of CH_4 (mL); φ_{CH4} is the CH_4 concentration (%); q is the total flow of mixed gas (mL); μ is the replacement ratio (dimensionless); $Q^T{}_{N2}$ is the total injected amount of N_2 (mL); t is time (min).

According to the experimental results, the η was 52.3%, 55.9%, 62.9%, 79.9%, and 85.2%, respectively, under different injection pressures. With increase in pressure, the η

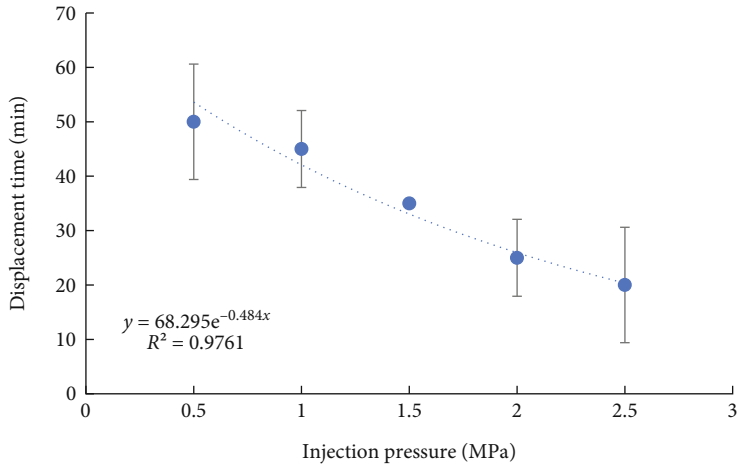

Figure 8: Displacement time under different pressures.

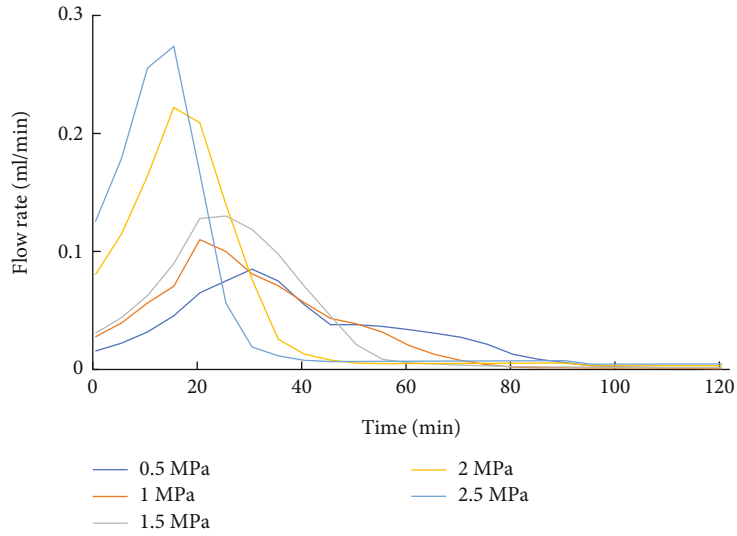

Figure 9: The flow rate of CH_4 under different injection pressures.

increased by 6.8%, 20.2%, 52.7%, and 62.9%, respectively. The μ in different pressures was 10.9, 10.2, 9.1, 7.2, and 6.7, respectively. With increase in pressure, the μ decreased by 6.4%, 16.5%, 33.9%, and 38.5%, respectively. It can be concluded that η increased with the increase of injection pressure. And the greater the pressure, the more significant the η increased. The maximum increase was more than 60%. The μ decreased with increase in pressure. The maximum decrease of μ was more than 38%.

3.5. Flow Rate of CH_4 and Accumulated Production of CH_4. It can be seen from Figure 9 that the maximum flow rate of CH_4 was 0.085 mL/min, 0.110 mL/min, 0.130 mL/min, 0.222 mL/min, and 0.273 mL/min, respectively, at the level of 0.5 MPa, 1 MPa, 1.5 MPa, 2 MPa, and 2.5 MPa. The regression curve appeared wave top under different injection pressures. The greater the injection pressure, the sharper the waveform. While the less the injection pressure, the wider the waveform. According to the experimental results, the flow rate of CH_4 decreased after an initial increase under different injection pressures. The peak value of the flow rate of CH_4 increased with the injection pressure. But the flow rate of CH_4 decreased rapidly at the pressure above 1.5 MPa. This indicated that the N_2 flowed easily in pores and fractures with high injection pressure so that the breakthrough time decreased. But the N_2 do not remain in the coal matrix at high injection pressure. Therefore, the coal matrix cannot effectively adsorb N_2 at a pressure above 1.5 MPa, which results in a large amount of CH_4 remaining in the coal.

It can be seen from Figure 10 that the accumulated production of CH_4 was 3.59 mL, 3.91 mL, 4.39 mL, 5.58 mL, and 5.94 mL, respectively, at the level of 0.5 MPa, 1 MPa, 1.5 MPa, 2 MPa, and 2.5 MPa. The results showed that the accumulated production of CH_4 increased with the increase in injection pressure. However, the increase of accumulated

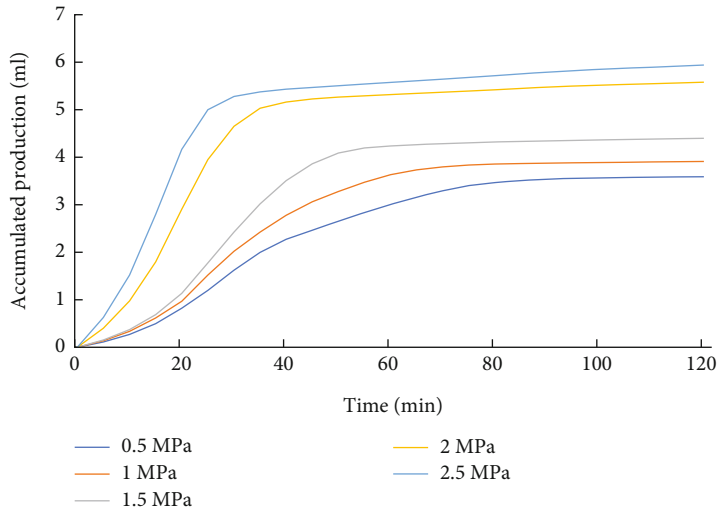

Figure 10: Accumulated CH_4 production under different pressures.

Table 2: Data standardization results under different pressures.

Code	Injection pressure (MPa)	Displacement efficiency (%)	Standardized processing	Replacement ratio	Standardized processing
1	0.5	52.3	0	10.9	1
2	1	55.9	0.89	10.2	0.16
3	1.5	62.9	0.32	9.1	0.57
4	2	79.9	0.16	7.2	0.88
5	2.5	85.2	1	6.7	0

production of CH_4 decreased at the injection pressure above 2 MPa. This indicated that the amount of CH_4 displaced by N_2 increased with the increase of injection pressure. The increase of injection pressure will increase the permeability of the coal so that it is easier for the gas to migrate in the seepage channel. It can be concluded that at the beginning, N_2 diffused from fractures to micropores, and competitive adsorption occurred. A large amount of CH_4 had been replaced due to a decrease of the partial pressure of CH_4. After reaching the critical time, CH_4 desorption and N_2 adsorption reached dynamic equilibrium. Therefore, the production of CH_4 will no longer increase. According to the displacement efficiency, the injection pressure can be divided into three stages. At the range of 0.5~1 MPa, it was the low-efficiency stage, and the displacement efficiency was about 50%; at the range of 1~2 MPa, it was the medium efficiency stage, and the displacement efficiency was about 60%; at the range of 2~2.5 MPa, it was the high-efficiency stage, and the displacement efficiency was 70~85%.

3.6. N_2 Injection Pressure. In the experiment, the displacement efficiency and replacement ratio were obtained according to different evaluation indicators. The two parameters cannot be directly compared and analyzed. In order to eliminate the impact of the difference in the dimension and value range among the indicators, it was necessary to carry out a standardization process and scale the parameters according to the proportion. The minimum-maximum normalization of the parameters, also known as discrete normalization, maps the parameter's value to (0, 1) according to the linear transformation of the original data according to formula (2). The data processing results are shown in Table 2.

$$A_Z = \frac{A - \min}{\max - \min}. \tag{2}$$

It can be seen from Figure 11 that there is a crossover point between the displacement efficiency and replacement ratio with different injection pressures after the discrete standardization treatment of the two parameters. The injection pressure corresponding to the crossover point was 1.6 MPa, and the displacement efficiency was 45%. Theoretically, the injection pressure corresponding to the crossover point was the most economical. The displacement efficiency increased with the increase of the injection pressures, while the replacement ratio decreased with the increase of the injection pressures. Figure 11 shows that the displacement efficiency was low while the replacement ratio is relatively high at the range of 0.5~1.6 MPa. This indicated that the amount of N_2 required for the displacement of CH_4 per unit volume was large. This pressure range was not ideal from a technical and economic perspective. At the range of 1.6~2 MPa, the displacement efficiency was high, but the replacement ratio is gradually reduced. This indicated that the amount of N_2 required for the displacement of unit volume of CH_4 was low. At injection pressure above 2 MPa, the increase rate of displacement efficiency was low, and the decrease rate of displacement ratio was reduced. This

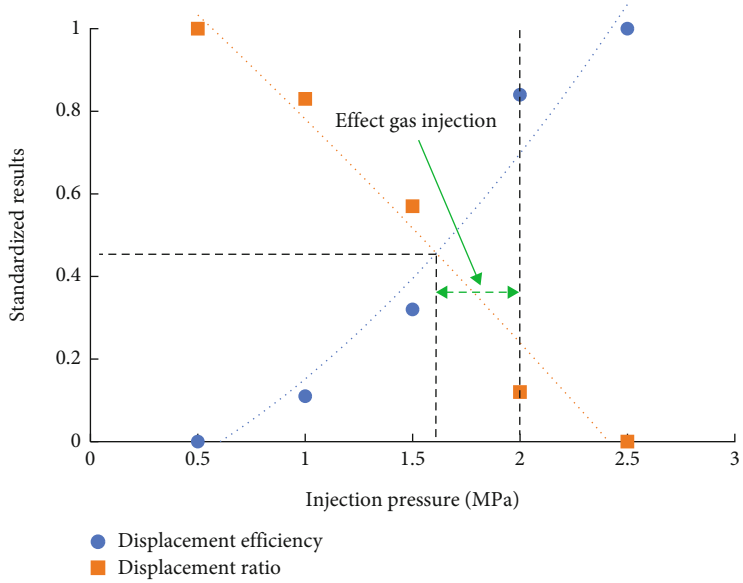

Figure 11: Displacement efficiency and displacement ratio under different pressures.

indicated that the flow velocity of N_2 and free CH_4 increased with the increase of injection pressure. At the same time, the displacement efficiency increased with the increase of injection pressure. Therefore, more N_2 enters into the tiny pores of the coal matrix so that more adsorbed CH_4 was displaced in the pores. The larger the amount of CH_4 displaced, the smaller the replacement ratio. When the injection pressure is greater than 2 MPa, the change rate of displacement efficiency and replacement ratio decreases with the increase of injection pressure, which shows that the influence of injection pressure on displacement efficiency and replacement ratio is weakened.

4. Discussion

The displacement of CH_4 by N_2 is a dynamic process. Most of the researchers [17, 23, 32] divide the process into three stages. This is also verified by our experimental results. According to our experimental results, the variation rate of the concentration of CH_4 showed a trend of increase before decrease. It was believed that the free CH_4 in the coal samples would be driven away to the outlet first after N_2 was injected into the coal samples. When the concentration of CH_4 in the fractures and macropores decreased, the desorbed CH_4 in the coal surface increased. Then, a large number of empty adsorption sites would be left [8, 17]. The N_2 would diffuse into the coal surface with the increase of injection [13]. Thus, the N_2 molecules would collide with the empty adsorption sites which had not yet adsorbed CH_4 molecules [27]. Then, the N_2 molecules would occupy the empty adsorption sites. In addition, the partial pressure of CH_4 decreased with the injection of N_2. The partial pressure of CH_4 would promote the desorption of CH_4, which provides more adsorption sites for N_2 [43]. However, the adsorption of N_2 molecules on the coal surface was weak. The coal surface cannot absorb N_2 molecules anymore with continuous injection. Then, the injected N_2 would migrate directly to the outlet of the coal samples. At the inception of stage II, the concentration of CH_4 produced increased rapidly because there was a large amount of free CH_4 in the fractures. Then, both of the free CH_4 and adsorbable CH_4 in the coal samples were decreased. Thus, the rate of decrease of CH_4 concentration was increased first and then decreased.

Gas extraction undergoes a desorption-diffusion-seepage process [44]. The transport of N_2 and CH_4 after N_2 injection into coal seams is an interactive process. After the injection of N_2, the injected gas occupies a certain space and bears part of the pore pressure. The number of adsorption sites in coal is fixed. The number of adsorption sites occupied by the injected gas increases which results to the decrease of CH_4-occupied adsorption sites [43]. This means that the increased partial pressure after N_2 injection can promote the desorption of CH_4. In addition, after gas injection, the reservoir pressure increases while the effective stress decreases. Thus, the permeability of the coal increases, which is conducive to the transport of CH_4 [42]. These two points indicate that the higher the injection pressure, the more methane is produced. However, the results of Figure 10 show that when the injection pressure is increased to a certain level, the methane output increases insignificantly. We believe that the bidirectional diffusion processes of gases influence the output of methane. The flow rate of the injected gas increases as the injection pressure increases. When the flow rate of injection gas is too fast, the injected gas cannot diffuse sufficiently into the coal matrix, resulting in reduced methane production. Thus, there is a specific pressure range which is beneficial to the production of methane.

5. Conclusion

(1) The whole process of CH_4 displacement by N_2 is a dynamic process. It can be divided into three stages:

stage I (original equilibrium stage); stage II (dynamic balance stage); stage III (new equilibrium stage). The concentration of CH_4 and N_2 presented an opposite variation trend, and the variation rate of CH_4 and N_2 increased first and then decreased

(2) Both of the breakthrough time and displacement time were negatively correlated with the injection pressures. The maximum flow rates of CH_4 increased with the increased injection pressures. But the attenuating tendency of flow rates of CH_4 was obvious with the increased injection pressures. The accumulated production of CH_4 increased with the increased injection pressures

(3) The displacement efficiency increased with the increased injection pressures while the replacement ratio decreased with the increased injection pressures. The effective injection pressure range for the test samples was 1.6~2 MPa from a technical and economic perspective

Data Availability

The data used to support the findings of this study are available from the corresponding author upon request.

Conflicts of Interest

The authors declare no conflict of interest.

Authors' Contributions

Z.A. and S.L. were responsible for the conceptualization. S.X. was responsible for the methodology. Z.A. was responsible for the formal analysis. Z.A. was responsible for the resources. Z.A. was responsible for the writing—original draft preparation. S.L. was responsible for the writing—review and editing. S.L. was responsible for the visualization. H.Z. was responsible for the supervision. S.L. was responsible for the project administration. All authors have read and agreed to the published version of the manuscript.

Acknowledgments

This research was funded by the National Natural Science Foundation of China (No. 51974161).

References

[1] Y. Qin, T. A. Moore, J. Shen, Z. Yang, Y. Shen, and G. Wang, "Resources and geology of coalbed methane in China: a review," *International Geology Review*, vol. 60, pp. 777–812, 2018.

[2] Y. Cao, D. He, and D. C. Glick, "Coal and gas outbursts in footwalls of reverse faults," *International Journal of Coal Geology*, vol. 48, no. 1-2, pp. 47–63, 2001.

[3] M. Qian, J. Xu, and X. Miao, "Gully-specific debris flow hazard assessment in China," *Journal of China University of Mining and Technology*, vol. 13, no. 2, pp. 112–118, 2003.

[4] C. Wu, C. Yuan, G. Wen, L. Han, and H. Liu, "A dynamic evaluation technique for assessing gas output from coal seams during commingling production within a coalbed methane well: a case study from the Qinshui Basin," *International Journal of Coal Science & Technology*, vol. 7, no. 1, pp. 122–132, 2020.

[5] Q. Zou, H. Liu, Z. Cheng, T. Zhang, and B. Lin, "Effect of slot inclination angle and borehole-slot ratio on mechanical property of pre-cracked coal: implications for ECBM recovery using hydraulic slotting," *Natural Resources Research*, vol. 29, pp. 1705–1729, 2020.

[6] L. Zhang, S. Lu, C. Zhang, and S. Chen, "Effect of cyclic hot/cold shock treatment on the permeability characteristics of bituminous coal under different temperature gradients," *Journal of Natural Gas Science and Engineering*, vol. 75, p. 103121, 2020.

[7] C. Fan, M. Luo, S. Li, H. Zhang, Z. Yang, and Z. Liu, "A thermo-hydro-mechanical-chemical coupling model and its application in acid fracturing enhanced coalbed methane recovery simulation," *Energies*, vol. 12, no. 4, p. 626, 2019.

[8] L. Zhang, S. Chen, C. Zhang, X. Fang, and S. Li, "The characterization of bituminous coal microstructure and permeability by liquid nitrogen fracturing based on CT technology," *Fuel*, vol. 262, article 116635, 2020.

[9] M. Lu and L. D. Connell, "Coal seam failure during primary/enhanced gas production: how failure develops in fields," *International Journal of Coal Geology*, vol. 221, p. 103432, 2020.

[10] C. Fan, S. Li, D. Elsworth, J. Han, and Z. Yang, "Experimental investigation on dynamic strength and energy dissipation characteristics of gas outburst-prone coal," *Energy Science & Engineering*, vol. 8, no. 4, pp. 1015–1028, 2020.

[11] Z. Liu, Y. Cheng, Y. Wang, L. Wang, and W. Li, "Experimental investigation of CO_2 injection into coal seam reservoir at in-situ stress conditions for enhanced coalbed methane recovery," *Fuel*, vol. 236, pp. 709–716, 2019.

[12] B. Brattekås and M. Haugen, "Explicit tracking of CO_2-flow at the core scale using micro-positron emission tomography (μPET)," *Journal of Natural Gas Science and Engineering*, vol. 77, p. 103268, 2020.

[13] N. Fan, J. Wang, C. Deng, Y. Fan, Y. Mu, and T. Wang, "Numerical study on enhancing coalbed methane recovery by injecting N2/CO2mixtures and its geological significance," *Energy Science & Engineering*, vol. 8, no. 4, pp. 1104–1119, 2020.

[14] M. Asif, M. Pillalamarry, D. C. Panigrahi, P. Naveen, and K. Ojha, "Measurement of coalbed gas content of Indian coalfields: a statistical approach," *International Journal of Oil, Gas and Coal Technology*, vol. 25, no. 1, pp. 73–88, 2020.

[15] R. Wang, Q. Wang, Q. Niu, J. Pan, H. Wang, and Z. Wang, "CO_2 adsorption and swelling of coal under constrained conditions and their stage-change relationship," *Journal of Natural Gas Science and Engineering*, vol. 76, p. 103205, 2020.

[16] C. R. Clarkson, A. Vahedian, A. Ghanizadeh, and C. Song, "A new low-permeability reservoir core analysis method based on rate-transient analysis theory," *Fuel*, vol. 235, pp. 1530–1543, 2019.

[17] X. Zhang and P. G. Ranjith, "Experimental investigation of effects of CO_2 injection on enhanced methane recovery in coal seam reservoirs," *Journal of CO2 Utilization*, vol. 33, pp. 394–404, 2019.

[18] A. S. Ranathunga, M. S. A. Perera, P. G. Ranjith, and C. Wei, "An experimental investigation of applicability of CO_2 enhanced coal bed methane recovery to low rank coal," *Fuel*, vol. 189, pp. 391–399, 2017.

[19] S. Liu, C. Zhu, B. Lin, and T. Liu, "The effect of spatial distribution mode of hydraulic slotting on pressure relief and permeability enhancement of the coal seam," *Journal of Mining and Safety Engineering*, vol. 37, pp. 983–990, 2020.

[20] Y. Yang, Q. Xu, X. Li et al., "Pore-scale simulation of gas-water two-phase flow in volcanic gas reservoir based on volume of fluid method," *Journal of Natural Gas Science and Engineering*, vol. 106, p. 104733, 2022.

[21] S. Zhu and A. Salmachi, "Flowing material balance and rate-transient analysis of horizontal wells in under-saturated coal seam gas reservoirs: a case study from the Qinshui Basin, China," *Energies*, vol. 14, no. 16, p. 4887, 2021.

[22] S. Chen, J. Zhang, D. Yin, X. Cheng, and N. Jiang, "Relative permeability measurement of coal microchannels using advanced microchip technology," *Fuel*, vol. 312, article 122633, 2022.

[23] H. Wang, Q. Ran, X. Liao, X. Zhao, M. Xu, and P. Fang, "Study of the CO_2 ECBM and sequestration in coalbed methane reservoirs with SRV," *Journal of Natural Gas Science and Engineering*, vol. 33, pp. 678–686, 2016.

[24] X. Liu, C. Liu, and G. Liu, "Dynamic behavior of coalbed methane flow along the annulus of single-phase production," *International Journal of Coal Science & Technology*, vol. 6, no. 4, pp. 547–555, 2019.

[25] L. Zhang, Z. Ye, M. Li, C. Zhang, Q. Bai, and C. Wang, "The binary gas sorption in the bituminous coal of the Huaibei coalfield in China," *Adsorption Science and Technology*, vol. 36, pp. 1612–1628, 2018.

[26] D. J. Black, "Review of current method to determine outburst threshold limits in Australian underground coal mines," *International Journal of Mining Science and Technology*, vol. 29, no. 6, pp. 859–865, 2019.

[27] S. N. Longinos, L. Wang, and R. Hazlett, "Advances in cryogenic fracturing of coalbed methane reservoirs with LN2," *Energies*, vol. 15, no. 24, p. 9464, 2022.

[28] S. N. Longinos, A. Serik, D. Zhang, L. Wang, and R. Hazlett, "Experimental evaluation of liquid nitrogen fracturing on the coal rocks in Karaganda Basin, Kazakhstan," *Arabian Journal for Science and Engineering*, pp. 1–16, 2023.

[29] S. N. Longinos, A. Dillinger, L. Wang, and R. Hazlett, "Uniaxial compressive strength (UCS) and SEM study of liquid nitrogen for waterless hydraulic fracturing in coalbed methane reservoirs of Karaganda Basin in Kazakhstan," *Gas Science and Engineering*, vol. 115, article 204998, 2023.

[30] Y. Wu, J. Liu, Z. Chen, D. Elsworth, and D. Pone, "A dual poroelastic model for CO_2-enhanced coalbed methane recovery," *International Journal of Coal Geology*, vol. 86, pp. 177–189, 2011.

[31] H. Kumar, D. Elsworth, J. P. Mathews, J. Liu, and D. Pone, "Effect of CO_2 injection on heterogeneously permeable coalbed reservoirs," *Fuel*, vol. 135, pp. 509–521, 2014.

[32] E. Ozdemir, "Modeling of coal bed methane (CBM) production and CO_2 sequestration in coal seams," *International Journal of Coal Geology*, vol. 77, no. 1-2, pp. 145–152, 2009.

[33] X. Huang, L. Zhang, R. Zhang, X. Chen, Y. Zhao, and S. Yuan, "Numerical simulation of gas-liquid two-phase flow in the micro-fracture networks in fractured reservoirs," *Journal of Natural Gas Science and Engineering*, vol. 94, article 104101, 2021.

[34] C. J. Seto, K. Jessen, and F. M. Orr, "A four-component two-phase flow model for CO_2 storage and enhanced coalbed methane recovery," in *Paper presented at the SPE Annual Technical Conference and Exhibition*, San Antonio, Texas, USA, 2006.

[35] T. Xia, F. Zhou, J. Liu, S. Hu, and Y. Liu, "A fully coupled coal deformation and compositional flow model for the control of the pre-mining coal seam gas extraction," *International Journal of Rock Mechanics and Mining Sciences*, vol. 72, pp. 138–148, 2014.

[36] S. R. Reeves, D. W. Davis, and A. Y. Oudinot, "A technical and economic sensitivity study of enhanced coalbed methane recovery and carbon sequestration in coal," *Doe Topical Report*, vol. 65, pp. 58–60, 2013.

[37] W. D. Gunter, M. J. Mavor, and J. R. Robinson, "CO_2 storage and enhanced methane production: field testing at Fenn-Big Valley, Alberta, Canada, with application," *Greenhouse Gas Control Technologies*, vol. I, pp. 413–421, 2005.

[38] W. Z. Zhao, X. B. Su, D. P. Xia, S. H. Hou, Q. Wang, and Y. X. Zhou, "Enhanced coalbed methane recovery by the modification of coal reservoir under the supercritical CO_2 extraction and anaerobic digestion," *Energy*, vol. 259, article 124914, 2022.

[39] J. Shi, S. Durucan, and M. Fujioka, "A reservoir simulation study of CO_2 injection and N_2 flooding at the Ishikari coalfield CO_2 storage pilot project, Japan," *International Journal of Greenhouse Gas Control*, vol. 2, no. 1, pp. 47–57, 2008.

[40] S. Yamaguchi, K. Ohga, M. Fujioka, and M. Nako, "Field test and history matching of the CO_2 sequestration project in coal seams in Japan," *International Journal of the Society of Materials Engineering for Resources*, vol. 13, no. 2, pp. 64–69, 2006.

[41] S. Cho, S. Kim, and J. Kim, "Life-cycle energy, cost, and CO_2 emission of CO_2-enhanced coalbed methane (ECBM) recovery framework," *Journal of Natural Gas Science and Engineering*, vol. 70, article 102953, 2019.

[42] S. Harpalani and A. Mitra, "Impact of CO_2 injection on flow behavior of coalbed methane reservoirs," *Transport in Porous Media*, vol. 82, no. 1, pp. 141–156, 2010.

[43] X. Du, D. Pang, Y. Cheng et al., "Adsorption of CH_4, N_2, CO_2, and their mixture on montmorillonite with implications for enhanced hydrocarbon extraction by gas injection," *Applied Clay Science*, vol. 210, article 106160, 2021.

[44] P. Ji, Y. Guo, L. Zhang, X. Kong, X. Wang, and Y. Zhou, "Research on gas pre-draining in coal roadway strips by combined ordinary drilling and directional drilling," *Industrial and Mining Automation*, vol. 47, pp. 61–66, 2021.